Enhancement of charge carrier transport by doping PVK-based photoconductive polymers with $LiNbO_3$ nanocrystals

S. Mansurova
National Institute for Astrophysics, Optics, and Electronics, AP 51 y 216, Puebla 72000, Mexico

K. Meerholz and E. Sliwinska
Institute of Physical Chemistry, University of Cologne, Luxemburger Str. 116, D-50939 Cologne, Germany

U. Hartwig and K. Buse
Institute of Physics, University of Bonn, Wegelerstr. 8, D-53115 Bonn, Germany
(Received 9 January 2009; published 29 May 2009)

The photoconductive properties of a hybrid material based on poly(N-vinylcarbazole) (PVK) doped with nanoparticles of lithium niobate ($LiNbO_3$) have been studied. The experiments were carried out using modulated photocurrent and non-steady-state photo-emf techniques at 633 nm wavelength. The photoconductivity of the composite increases remarkably with the nanoparticle content. This growth is related to larger drift lengths of the photoholes at higher nanoparticle concentrations. The reason for this enhancement is an increase in the effective photohole lifetime due to trapping of electrons on the nanoparticles and creation of recombination barriers at the polymer/nanoparticle interface.

DOI: 10.1103/PhysRevB.79.174208 PACS number(s): 81.07.Pr, 72.20.Jv, 73.63.Bd, 82.35.Np

I. INTRODUCTION

Nanocrystal technology enables the realization of inorganic-organic hybrid composites, where nanosized particles are embedded into a conductive organic matrix.[1,2] In recent years, there has been a substantial rise of interest regarding the use of nanoparticles (NP) as dopants in composites based on polymers or liquid crystals, which may be utilized as a material for photovoltaic devices (solar cells),[3] light emitting diodes,[4] or holographic storage media.[5,6] Such a composite provides a number of important advantages as compared with bulk homogeneous materials. First, the properties of the NPs (Refs. 7–10) can be modified in a wide range by controlling their composition, size, and interface with the matrix. Second, the interface area between the polymer and the NP is very large due to the very high surface/volume ratio of the NPs. This enables efficient exciton separation at the interface which, as a consequence, may enhance charge generation,[11] as well as charge transport.[12] Third, the photoelectric properties of the polymeric phase can be varied via doping with small organic molecules. Finally, the mechanical properties of the hybrid material can be easily optimized by varying the polymer composition.

Here, we report on the investigation of a composite based on copper-doped $LiNbO_3$ embedded into the well studied photoconductive poly(N-vinylcarbazole) (PVK) matrix.[13] The choice of $LiNbO_3$ as the inorganic component is motivated by its outstanding properties. $LiNbO_3$ is a ferroelectric crystal showing the bulk photovoltaic effect, where the light-induced electric field, aligned along the crystallographic c axis, can be as high as 10 $V/\mu m$.[14,15] This induced polarization can modify the local field around the nanoparticles and stimulate the separation of photoexcited electron-hole pairs in the polymer matrix. Furthermore, in poled hybrid material the $LiNbO_3$ NPs can also act as the electro-optic or nonlinear optical component instead of the commonly used organic dye molecules. This may allow using the composite for photorefractive recording[16] or optical frequency conversion and, finally, the piezoelectric and pyroelectric properties of $LiNbO_3$ can lead to additional interesting applications in sensors and actuators. For all these applications the knowledge of the physical mechanisms, which governs the charge transport in such hybrid organic-inorganic composites, is the key issue. Here we present a study of the photoconductive properties of a PVK-$LiNbO_3$ hybrid material by modulated photocurrent and non-steady-state photo-emf techniques.

II. EXPERIMENTAL METHODS

A. Sample preparation

The organic host consists of a photoconductor PVK matrix sensitized with 2,4,7-trinitrofluorenone (TNF). In order to enable the film preparation, the plasticizer *N*-ethylcarbasole (ECZ) was added. In one experiment, investigating the influence of the acceptor strength, TNF was replaced by 2,4,7-trinitromalononitrile (TNFM).

$LiNbO_3$ wafers were doped with Cu by indiffusion. The copper concentration and Cu^+/Cu^{2+} ratio amount 10^{19} cm^{-3} and 0.2, respectively. Nanocrystalline $LiNbO_3$ particles were obtained by milling of the wafers (ball mill, 20 h milling time). The size of the nanocrystals was determined by dynamic laser-light scattering measurements and is about 20 nm. In order to increase the compatibility of the polar crystals with the relatively nonpolar polymer matrix, the nanocrystals were treated with dimethyldichlorosilane in 1,1,1-trichlorethane, a silanization agent, which reacts with the dangling oxygen bonds on the $LiNbO_3$ surface.[17] This procedure ultimately yields a monolayer of the agent on the $LiNbO_3$ surface. For comparison, on a bulk $LiNbO_3$ wafer this treatment leads to a substantial change in the contact angle for water from $\approx 30°$ on the untreated to $\approx 70°$ on the

treated sample, indicating the reduced polarity of the crystal surface. For mixing, all components were dispersed in dichloromethane and the solvent was then allowed to evaporate. Uniform films were fabricated by sandwiching the composite between two transparent indium-tin-oxide-coated glass substrates at elevated temperature using glass spacer beads to adjust the film thickness to be 105 μm.

B. Modulated photoconductivity

The photoconductive properties of the polymeric matrix were studied by means of modulated photocurrent and non-steady-state photo-emf techniques. In modulated photocurrent experiments the dc biased sample is homogeneously illuminated by a laser beam of a periodically varied intensity (oscillation frequency Ω). A modulated photoconductivity is created, and application of an external electric field E_0 yields the modulated photocurrent density with the amplitude:[18]

$$j_{\mathrm{ph}}^{\Omega} = E_0 \sigma_0 \frac{1}{\sqrt{1+\Omega^2 \tau_{\mathrm{ph}}^2}}. \tag{1}$$

Here $\sigma_0 = eg\mu\tau$ is the average photoconductivity of the sample, e is the elementary charge, g is the charge carrier generation rate, μ is the free-carrier mobility, and τ is the photocarrier lifetime. The characteristic time τ_{ph} is the photoconductivity response time, which in some cases (e.g., in the presence of shallow traps) may differ from the photocarrier lifetime. Thus, measuring the frequency response of the photocurrent J_{ph}^{Ω} yields the photoconductivity response time.

C. Non-steady-state photo-emf

A detailed description of the non-steady-state photo-emf technique, based on detection of an alternating current induced in a photoconductive sample by a vibrating interference pattern, can be found, e.g., in Ref. 19. Illumination of the photoconductive sample with a sinusoidal interference pattern with period length Λ and effective contrast m gives rise to a grating of photoexcited mobile carriers, e.g., holes. Such an interference pattern can be obtained by superimposing two coherent plane waves. Redistribution of the mobile charges through drift or diffusion and their subsequent trapping by deep centers yields a spatially inhomogeneous space-charge field E_{sc} inside the sample. In addition, a sinusoidal phase modulation with amplitude Δ and frequency Ω is introduced in one of the recording beams. This causes an oscillation of the interference pattern. The interaction of the relatively stable space-charge-field grating with the moving free-carrier grating generates an alternating current that flows through the short-circuited sample. The maximal current density amplitude[20]

$$j_{\text{p-emf}}^{\Omega} = m^2 \frac{J_1(\Delta) J_0(\Delta)}{2} \sigma_0 \frac{E_D(1+K^2 L_D^2) - K L_0 E_0}{(1+K^2 L_D^2)^2 + K^2 L_0^2} \tag{2}$$

is observed when the oscillation frequency of the interference pattern is larger than the reciprocal space-charge grating buildup time τ_{sc}^{-1}, but smaller than the reciprocal photocarrier lifetime τ^{-1}, i.e., in the frequency range $\tau_{\mathrm{sc}}^{-1} \ll \Omega \ll \tau^{-1}$. Here $J_{1,0}(\Delta)$ is the Bessel function of the corresponding order, E_0 is the external dc field, $E_D = K(D/\mu)$ is the so-called diffusion field, $K = 2\pi/\Lambda$ is the spatial frequency of the interference pattern, D is the diffusion coefficient of mobile holes, and $L_D = (D\tau)^{-1/2}$ and $L_0 = \mu\tau E_0$ are the diffusion and drift lengths of the photocarriers. Note that the above expression was derived for a monopolar photoconductor with a single deep trap center, neglecting the dark conductivity and assuming no trap saturation.

Measuring the experimental dependences of the photo-emf current $J_{\text{p-emf}}^{\Omega}$ on the external dc field, the drift lengths of the photocarriers can be determined. Indeed, it can be seen from Eq. (2) that the photo-emf signal amplitude drops to zero when the diffusion and drift components of the space-charge grating compensate each other, i.e., when the condition

$$E_D(1+K^2 L_D^2) = K L_0 E_0 \tag{3}$$

is met. For large spatial periods of the interference fringes ($KL_D \ll 1$) this condition reduces to the equality of the drift and diffusion lengths $L_D = L_0$. Assuming the validity of the Einstein relation between the mobility and diffusion coefficient $D/\mu = k_B T/e$ (here k_B is the Boltzmann constant and T is the absolute temperature), the mobility-lifetime product $\mu\tau$ can be obtained from the position of the minimum $E_0' = \sqrt{\frac{k_B T}{e}\frac{1}{\mu\tau}}$.

D. Experimental procedure

In modulated photocurrent and photo-emf experiments the sample was illuminated by a He-Ne laser ($\lambda = 633$ nm) beam through the transparent electrodes. The size of the spot on the sample surface was 1.5 mm in diameter. Photo-emf experiments were performed in reflection geometry when two counterpropagating beams with nearly equal intensity illuminate the sample, creating an interference pattern with the period $\Lambda = \lambda/2n \approx 0.19$ μm. Our previous measurements of the diffusion length in PVK:TNF-based composites[21] show that the condition $KL_D \leq 1$ is fulfilled in this configuration. A sinusoidal phase modulation with the amplitude $\Delta = 0.5$ rad was introduced by an electro-optic modulator. The modulated photocurrent J_{ph}^{Ω} and photo-emf current $J_{\text{p-emf}}^{\Omega}$ signals were detected by a lock-in amplifier as a voltage drop at the load resistance R_L.

To assure the optimal modulation frequency regime in photo-emf measurements, i.e., $\tau_{\mathrm{sc}}^{-1} \ll \Omega \ll \tau^{-1}$, the $J_{\text{p-emf}}^{\Omega}(\Omega)$ dependence was obtained, and the two characteristic cut-off frequencies were determined: $\Omega_1/2\pi \approx 0.21$ Hz at the 0.95 W/cm^2 average light intensity and $\Omega_2/2\pi \approx 15$ Hz. In the following photo-emf experiments we used an intermediate modulation frequency $\Omega/2\pi = 2.0$ Hz located between these two.

III. EXPERIMENTAL RESULTS AND DISCUSSION

A. Modulated photoconductivity

The electric field dependences of the photocurrent measured in PVK:TNF:NP composites are depicted in Fig. 1. It can be seen that the photocurrent J_{ph}^{Ω} grows superlinearly as

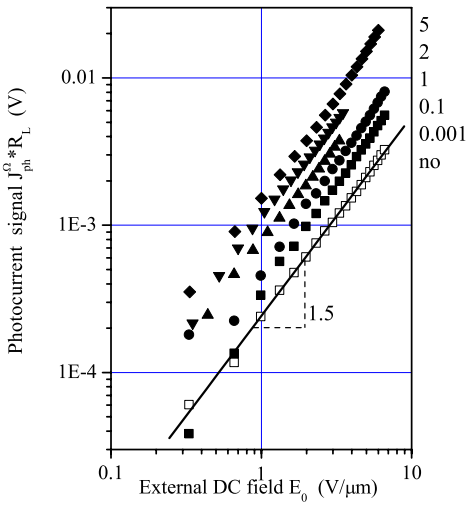

FIG. 1. (Color online) Experimental dependence of the ac photocurrent J^{Ω}_{ph} ($\Omega/2\pi$=1 Hz, I_0=0.95 W/cm^2, R_L=1 MΩ) on the dc field E_0 for different concentrations of $LiNbO_3$ NPs: □ 0; ■ 0.001; ● 0.1; ▲ 1, ▼2, ◆ 5 wt %.

$E_0^{1.5}$ for all concentrations of $LiNbO_3$ nanoparticles, indicating a dependence of the photoconductivity parameters on the electric field, either that of the generation rate due to the field-enhanced separation of geminate electron/hole pairs[22] or that of the carrier mobility,[13] which is typical for polymeric photoconductors.[23] The photocurrent amplitude increases for higher concentrations of NPs. It is worth to mention that no photocurrent was detected in samples which contain only PVK and $LiNbO_3$ NP, i.e., without TNF. When TNF was replaced by TNFM, the increase in the photoconductivity in the presence of the particles was strongly reduced (ca. factor 4).

The qualitative behavior of the photocurrent frequency dependence (Fig. 2) measured at E_0=3 V/μm and I_0 =0.95 W/cm^2 is well described by Eq. (1). The signal is frequency independent at low modulation frequencies and then starts to decay after some characteristic frequency Ω_0 $=\tau_{ph}^{-1}$. The decay at high modulation frequencies $\Omega \gg \Omega_0$,

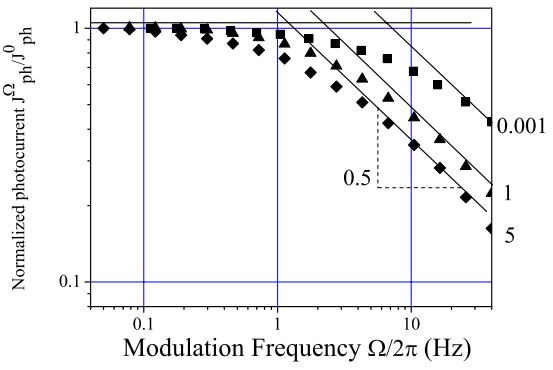

FIG. 2. (Color online) Dependence of the photocurrent J^{Ω}_{ph} on the modulation frequency $\Omega/2\pi$ (E_0=3 V/μm, I_0 =0.95 W/cm^2, R_L=1 MΩ) for different concentrations of $LiNbO_3$ NPs ■ 0.001, ▲ 1; ◆ 5 wt % normalized to the zero-frequency photocurrent value. The straight lines describe the asymptotic behavior at low and high frequency.

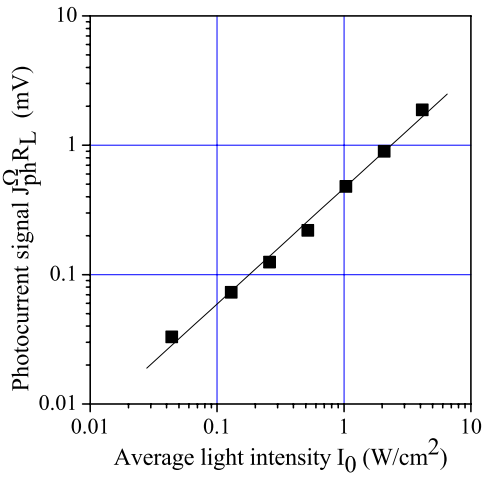

FIG. 3. (Color online) Modulated photocurrent J^{Ω}_{ph} vs the average light intensity I_0 ($\Omega/2\pi$=1 Hz, E_0=2 V/μm, R_L=1 MΩ) in the sample which contains 5 wt % of $LiNbO_3$ NPs.

however, is proportional to $\Omega^{-0.5}$, at least within the frequency range (limited by the small signal-to-noise ratio at high frequencies) where the experiment could be carried out. Such sublinear decay rate is slower than the linear Ω^{-1} decrease in the signal as predicted by Eq. (1), and it is typically observed in photoconductors where bimolecular recombination takes place. But measurements of the dependence of the photocurrent on the average light intensity I_0 (Fig. 3) show an almost linear ($\propto I_0^{0.9}$) growth which indicates that bimolecular recombination is unimportant in our sample. The slow frequency decay can be explained by a dispersion of the characteristic times due to the hopping transport typical for amorphous organic and inorganic materials.[24] The important observation is that the characteristic frequency Ω_0 decreases for higher NP content, which corresponds to an increase in the photoconductivity response time τ_{ph}. Variations in τ_{ph} can be explained usually by two factors:[25] either an influence of shallow traps—they increase the mean time which carriers contribute to the photoconductivity due to the process of trapping and thermal re-excitation—or a larger free-carrier recombination time. However, the first factor also affects the effective mobility of the free carriers in such a way that the $\mu\tau$ product and as a consequence also the photocurrent amplitude remain unchanged,[25] which is in contradiction to our experimental data (Fig. 1). This allows us to presume that the presence of the $LiNbO_3$ NPs enlarges the recombination time of the photocarriers.

B. Non-steady-state photo-emf

Figure 4 represents typical dependences of the non-steady-state photo-emf current on the external dc field at different NP content. It is seen that the photo-emf signal has a well pronounced minimum at low dc field, and then increases with growing E_0. We observe also that the minimum position shifts to lower dc fields at higher content of the $LiNbO_3$ NPs. Following Eq. (3), and for $KL_D \ll 1$, these data indicate that the drift length L_0 of the photoholes increases with a growing NP content. Figure 5 shows that both, pho-

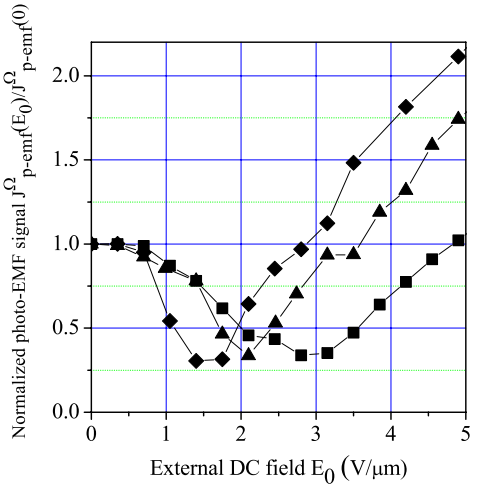

FIG. 4. (Color online) Non-steady-state photo-emf current $J^{\Omega}_{\text{p-emf}}$ vs the external dc field E_0 for different concentrations of $LiNbO_3$ NPs ■ 0.001, ▲ 1; ◆ 5 wt % ($\Omega/2\pi=2$ Hz, $I_0=0.95$ W/cm^2, $R_L=10$ MΩ). The photo-emf signal is normalized to the zero-field value. The solid lines are guides for the eyes.

tocurrent and drift length, increase in a similar way with the NP content, so it is clear that the main contribution to the increasing photoconductivity is due to a growth of the $\mu\tau$ product rather than due to an improved quantum efficiency of charge generation.

IV. MODEL OF CHARGE GENERATION AND TRANSPORT IN A PVK:TNF POLYMER COMPOSITE DOPED WITH $LiNbO_3$ NANOPARTICLES

A. Main experimental facts

Our experimental observations can be summarized as follows: (1) The presence of $LiNbO_3$ NPs enhances the photocurrent in the hybrid material. (2) This enhancement occurs due to an increased recombination time of the dominating photocarriers, which are holes in our material.[21] (3) The process of charge generation is unaffected by the presence of the NPs. Based on these facts we will discuss the processes responsible for charge generation and transport, which take place in the composite material.

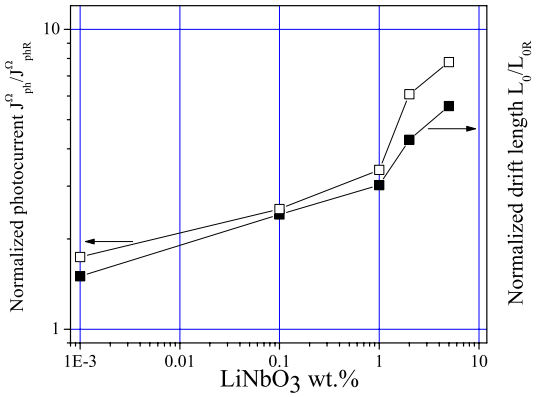

FIG. 5. (Color online) Concentration dependence of the normalized photocurrent amplitude $J^{\Omega}_{\text{ph}}/J^{\Omega}_{\text{phR}}$ (at $E_0=3.5$ V/μm and $\Omega/2\pi=1$ Hz) and of the normalized drift lengths L_0/L_{0R}. Here J^{Ω}_{phR} and L_{0R} are the values of photocurrent and drift length measured in the reference material without $LiNbO_3$ NPs.

B. Charge excitation

We will start from the last point (3) which indicates that the contribution of free charges generated inside the NPs to the photoconductivity of the composite is negligible. This is not surprising considering the absorption spectra of $LiNbO_3$ ($E_g=3.8$ eV) (Ref. 26). Fundamental (band-to-band absorption) takes place in the UV. Regarding the extrinsic absorption from the impurity levels, previous measurements of the absorption spectra[17] of a dispersion of Cu doped $LiNbO_3$ nanoparticles show an absorption peak at 425 nm, and at 633 nm the absorption is very low. Hence, upon illumination by visible light, generation of free charge carriers takes place mainly inside the organic matrix. The absorption of photons there leads to excitation of electrons at the PVK-TNF charge-transfer complex, followed by their transfer to the TNF molecule and generation of the hole on the PVK transport manifold.[12]

Once generated, the charges are separated due to drift and diffusion. It is known that the mobility of holes in a PVK:TNF mixture is orders of magnitude higher than the mobility of electrons, mainly due to the fact that the concentration of TNF molecules is too low to constitute an efficient charge transport manifold. It is usually assumed that mobile holes contribute to the conductivity, while slow (but still mobile) electrons—in other words negatively charged anion radicals—act as recombination centers.

C. Energy levels

As it is shown by the above experimental data, the incorporation of NPs enlarges the drift lengths of free holes due to an increased recombination time. In order to figure out the mechanism responsible for this effect, the electron and hole energy levels in the polymer host and in the nanocrystals as well as at the polymer-nanocrystal interface are needed. The spectrum of the organic component is determined by the position of the lowest unoccupied molecular orbital (LUMO) and the highest occupied molecular orbital (HOMO), while for the crystalline component the relevant energy levels are the conduction band (CB) and the valence band (VB). The separation of HOMO and LUMO levels from vacuum level E_v for organic constituents in our composite is well known from the literature: PVK HOMO=5.85 eV, TNF LUMO =4.3 eV.[27] The PVK LUMO level, as well as the TNF HOMO, is of no interest here because there are no charged species there. In the following discussion we will represent the organic PVK:TNF mixture as a homogeneous semiconductor, where PVK HOMO and TNF LUMO play the role of valence (VB_O) and conduction band (CB_O), respectively.

Regarding the inorganic component, represented by $LiNbO_3$ nanocrystals, the separation between CB_I and VB_I, i.e., the forbidden gap $E_g=3.8$ eV, is also known.[26] The resulting energy scheme now depends on the separation of CB_I from the vacuum level, i.e., on the nanocrystals electron af-

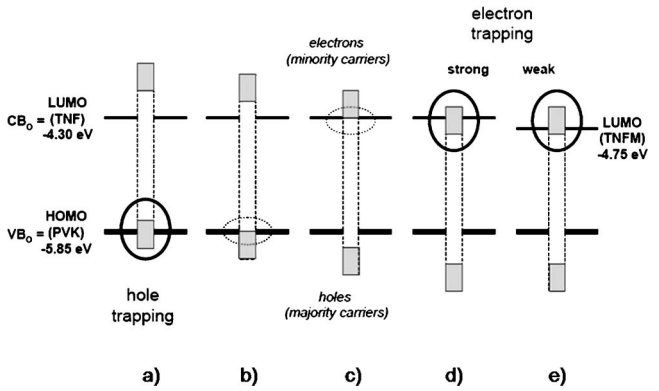

FIG. 6. [(a)–(d)] Energy scheme of the polymer: NP composite for different NP electron affinities; (e) electron affinity is the same as in case (d), but now the LUMO layer of the sensitizer is lowered.

finity χ_C. Some literature data indicate that pure bulk $LiNbO_3$ exhibits in vacuum a rather low electron affinity (−1.1 and −1.5 eV).[28,29] However, one has to be careful trying to apply directly this literature data to our material system. Indeed, Refs. 28 and 29 dealt with undoped bulk $LiNbO_3$ having a cleaned surface. In our case all these features are different: the sample is doped, the size is rather close to the limit where the structure and as a consequence the material parameters can be affected by low dimensionality, and the crystal surface is chemically pretreated.[30,31] The above-mentioned factors, as it was shown in Ref. 29, can alter the value of the electron affinity of the material significantly. In addition, one has also to keep in mind that $LiNbO_3$ is a polar material, i.e., there will be a significant difference of the electron affinity of the plus and minus faces orthogonal to the polar axis of this material. All this, in our opinion, renders direct application the above literature data to our system questionable. For this reason we will assume in the following analysis that the electron affinity of the inorganic component is unknown.

Figures 6(a)–6(d) illustrate four situations differing in the relative position of CB_I and CB_O: in the subfigures (a) and (b) the CB_I edge is located above, in subfigure (c) at the identical position, and finally in (d) below the CB_O. Note the difference of the width of the CB_I and VB_I in crystalline NP (where it amounts to 1 eV approximately), and of the CB_O and VB_O in organic components (where due to the weak intermolecular bonding the widths of the transport bands are at least 1 order of magnitude smaller).

The situation represented by Figs. 6(a) and 6(b) could apply, if we assume that the electron affinity of the NPs corresponds to that reported in literature for pure bulk $LiNbO_3$.[28,29] However, in this case the NPs would constitute potential wells for holes, acting as extended hole traps. This would result in a reduced concentration of mobile holes, which is in clear contradiction to our experimental data.

In the case represented by Fig. 6(c), i.e., when the CB_I and CB_O are aligned, the NPs would have no effect on the hole transport, which does not explain the observed increase in the recombination time. In contrast, the situation illustrated in Fig. 6(d), when $LiNbO_3$ CB_I lays below the TNF LUMO, may lead to the observed effect of a recombination

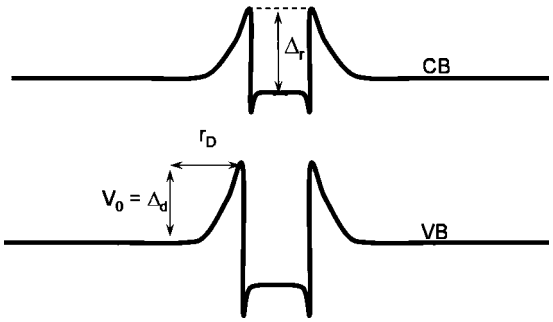

FIG. 7. Band bending effect and creation of the drift and recombination barriers in the polymer-nanocrystal composite under illumination.

time increase.[32,33] Indeed, in this case the NPs act as extended traps for electrons and represent a potential barrier for holes, leading to spatial separation of charges.

D. Charge transport

The key assumption of our analysis is that in the presence of the $LiNbO_3$ NPs the electrons from TNF^- anion radicals can be transferred to the adjacent NPs. If the edge of the CB_I of $LiNbO_3$ is located below the CB_O [Fig. 6(d)], this transition is energetically favorable. The captured electrons give rise to the accumulation of negative charge Q on the NPs. This charge is screened by an equal number of holes on carbazole units in the direct vicinity of a NP. The characteristic screening length is $r_D = \sqrt{\varepsilon\varepsilon_0 k_B T / e^2 N_T}$ and it is determined by the concentration of traps N_T in the polymer matrix. The charge separation leads to a bending of the band at the polymer/NP interface (Fig. 7). The amplitude of band bending V_0 varies logarithmically[32]

$$V_0 \cong k_B T \ln(l/r_D) \tag{4}$$

with the average distance between nanoparticles $l = N^{-1/3}$, where N is the NP content. Due to the Coulomb interaction between electrons trapped inside the negatively charged NP and positively charged holes, the HOMO level of PVK bends, which leads to the creation of a drift barrier for holes Δ_d (Fig. 7) with a height approximately equal to the band bending amplitude $\Delta_d \cong V_0$. As a result, the hole mobility decreases as $\mu_p \propto \exp(-\Delta_d / k_B T)$. The negatively charged NP and the positively charged cloud of holes around it form a compact core-shell structure.

In order to recombine, the electrons must overcome the recombination barrier Δ_r (Fig. 7) with a height, which is roughly equal to the energy separation between the edge of CB_O and CB_I. At room temperature the probability to be thermally activated is larger than the probability to tunnel through the barrier.[33] So, the electrons in the $LiNbO_3$ CB which acquire enough energy to reach the barrier edge are driven outside the NP by the electric field created by the separated charges. Once outside they can recombine with holes trapped on carbazoles surrounding the NP. For the mechanism of thermal activation the barrier increases the photohole recombination time exponentially:[32]

$$\tau_p \propto \exp(\Delta_r/3k_BT). \quad (5)$$

Thus, there are two factors which influence the photoconductivity in opposite ways: the presence of a drift barrier tends to decrease the overall photoconductivity (the drift velocity drops), while the recombination barrier increases it (the concentration of nonequilibrium holes grows). In general, if $\Delta_d < \Delta_r$, their joint influence will result in an increase in the photoconductivity[32,34] as observed experimentally.

Theoretical analysis performed in Ref. 32 reveals that for wide-gap inclusions, which is the case for $LiNbO_3$ with a forbidden gap $E_g=3.8$ eV larger than the 3.2 eV difference between PVK HOMO and LUMO levels, the photoconductivity increases due to the presence of inclusions as $N^{1/3}$, where N is the concentration of the NP. This occurs because the drift barrier for holes is reduced due to a decreased height of the potential profile V_0 [Eq. (4)] when the NP average separation distance becomes comparable with screening length $l \cong r_D$. The predicted $N^{1/3}$ growth was observed starting from NP concentrations >1 wt % (Fig. 5). This allows evaluating r_D as 10–15 nm, which for $\varepsilon_{PVK} \cong 3$ gives as an estimation of the trap concentration in the organic matrix of $N_T \cong 10^{17}$ cm^{-3}. The PVK:TNF mixture we used in our experiments is also commonly used in photorefractive recording, where the trap concentration N_T can be determined easily by measuring the photorefractive phase shift.[35] The above estimation of the trap density agrees very well with the literature value typical for this material class.[27,36]

This allows us to presume that the charge separation at the polymer/NP interface is indeed responsible for the enlargement of the recombination time with the NP concentration. At the microscopic level it implies that the electron affinity χ_c of $LiNbO_3$ NPs is larger than −4.3 eV (the LUMO level of TNF). This value deviates a lot from the literature values of the electron affinity of pure $LiNbO_3$ (−1.1 and −1.5 eV) mentioned above. Using TNFM as a sensitizer, which is a much stronger acceptor (LUMO level 0.45 eV deeper than for TNF), the relative difference between CB_I and CB_O is reduced [Fig. 6(e)], and we can expect that the effect of photocurrent enhancement by NP doping should also be reduced. This has been observed (Sec. III A), supporting our assumption.

The phenomena of separation of nonequilibrium charges due to an interfacial electric field and creation of recombination barriers in the system were studied in details in Refs. 32 and 34. As it was pointed out in Ref. 32, due to the fact that the organic component typically has a lower value of electron affinity than the embedded inorganic component, the situation we anticipated here and that is illustrated by the diagram Fig. 6(d) is rather general for most polymer-based hybrid composites. Indeed, for the most popular hole-transporting polymers—including polyphenylene vinylene (PPV), triphenyldiamine (TPD), and polyvinyl carbazole (PVK)—the electron affinity ranges from 2.3 to 2.6 eV.[37] This is less than typical electron affinities in CdS (3.8–4.8 eV) (Ref. 38), CdSe (~4.0 eV) (Ref. 38), or TiO_2 (~4.2 eV) (Ref. 39).

V. CONCLUSIONS

The photoconductive properties of an organic-inorganic hybrid material based on $LiNbO_3$ nanoparticles embedded into a PVK:TNF organic matrix have been investigated. The results demonstrate that $LiNbO_3$ NPs do not participate directly neither in charge generation, nor in transport of the dominating carriers (holes). Nevertheless, incorporation of NPs improves the photosensitivity due to a prolonged hole recombination time. This was explained by a model considering charge separation, followed by trapping on the NP, leading to the creation of a recombination barrier at the crystal-polymer interface. The key assumption of this model is that the relative position of the NP conduction band and of the LUMO level of the sensitizer (TNF or TNFM) is such that electron transfer from the surrounding sensitizer molecules into the nanocrystals is energetically favorable, converting them to extended electron traps. Due to the negative charge accumulation in the NPs, a recombination barrier for holes is created and the recombination lifetime of mobile holes is enlarged resulting in an overall increase in the photoconductivity.

ACKNOWLEDGMENTS

S.M. thanks the Alexander-von-Humboldt Foundation for financial support. Financial support by the DFG (Grants No. ME 1246/13 and No. BU 913/17) is gratefully acknowledged.

[1] Y. Wang, in *Kirk-Othmer Encyclopedia of Chemical Technology*, edited by J. Kroshwitz (Wiley, New York, 1996).
[2] Y. Wang and N. Herron, Chem. Phys. Lett. **200**, 71 (1992).
[3] V. L. Colvin, M. C. Schlamp, and A. P. Alivisatos, Nature (London) **370**, 354 (1994).
[4] N. C. Greenham, X. Peng, and A. P. Alivisatos, Phys. Rev. B **54**, 17628 (1996).
[5] J. G. Winiarz, L. Zhang, M. Lal, C. S. Friend, and P. N. Prasad, J. Am. Chem. Soc. **121**, 5287 (1999).
[6] E. Buchnev, A. Dyadyusha, M. Kaczmarek, V. Reshetnyak, and Y. Reznikov, J. Opt. Soc. Am. B **24**, 1512 (2007).
[7] B. O. Dabboussi, J. Rodriguez Viejo, F. V. Mikules, J. R. Heine, H. Mattoussi, R. Ober, K. F. Jensen, and M. G. Bawendi, J. Phys. Chem. B **101**, 9463 (1997).
[8] A. J. Eychmüller, J. Phys. Chem. B **104**, 6514 (2000).
[9] T. Trindade, P. O'Brien, and N. L. Pickett, Chem. Mater. **13**, 3843 (2001).
[10] S. H. Wang, S. H. Yang, C. L. Yang, Z. Li, J. Wang, and W. Ge, J. Phys. Chem. B **104**, 11853 (2000).
[11] B. O'Regan and M. Grätzel, Nature (London) **353**, 737 (1991).
[12] K. R. Choudhury, M. Samoc, A. Patra, and P. N. Prasad, J. Phys. Chem. B **108**, 1556 (2004).
[13] W. D. Gill, J. Appl. Phys. **43**, 5033 (1972).
[14] D. von der Linde, A. M. Glass, and K. F. Rodgers, Appl. Phys.

Lett. **25**, 155 (1974).
[15] M. Simon, St. Wevering, K. Buse, and E. Krätzig, J. Phys. D **30**, 144 (1997).
[16] P. Günter and J. P. Huignard, *Photorefractive Materials, Effect and Their Applications* (Springer Verlag, Berlin, 2006).
[17] J. R. Schwesyg, H. A. Eggert, K. Buse, E. Sliwinska, S. Khalil, M. Kaiser, and K. Meerholz, Appl. Phys. B: Lasers Opt. **89**, 15 (2007).
[18] A. Gerwens, K. Buse, and E. Krätzig, Ferroelectrics **202**, 203 (1997).
[19] S. Stepanov, in *Photo-Electromotive-Force Effect in Semiconductors in Handbook on Advanced Electronics and Photonics Materials*, edited by H. S. Nalwa (Academic, San Diego, 2001).
[20] I. A. Sokolov and S. I. Stepanov, J. Opt. Soc. Am. B **10**, 1483 (1993).
[21] S. Mansurova, S. Stepanov, R. Ramos Garcia, V. Camacho Pernas, F. Gallego-Gomez, E. Mecher, and K. Meerholz, Phys. Rev. B **69**, 193203 (2004).
[22] P. M. Borsenberger and A. I. Ateya, J. Appl. Phys. **49**, 4035 (1978).
[23] P. M. Borsenberger and D. Weiss, *Organic Photoreceptors for Xerophotography* (Dekker, New York, 1998).
[24] B. Sturman, E. Podivilov, and M. Gorkunov, Phys. Rev. Lett. **91**, 176602 (2003).
[25] A. Rose, *Concepts in Photoconductivity and Allied Problems* (Interscience Publishers, New York, 1963).
[26] L. Kovacs, G. Ruschhaupt, K. Polgar, and G. Corradi, Appl. Phys. Lett. **70**, 2801 (1997).
[27] R. Bittner and K. Meerholz, in *Photorefractive Materials and Their Applications 2*, edited by P. Günter and J. P. Huignard (Springer, New York, 2007).
[28] W.-C. Yang, B. J. Rodriguez, A. Gruverman, and R. J. Nemanich, Appl. Phys. Lett. **85**, 2316 (2004).
[29] A. A. Akhayan and A. N. Brozdnichenko, Sov. Phys. Solid State **25**, 1990 (1983).
[30] W. L. Zhong, B. Jiang, P. L. Zhang, J. M. Ma, H. M. Cheng, and Z. H. Yang, J. Phys.: Condens. Matter **5**, 2619 (1993).
[31] K. Uchino, E. Sadanaga, and T. Hirose, J. Am. Ceram. Soc. **72**, 1555 (1989).
[32] A. Shik, H. Ruda, and E. H. Sargent, J. Appl. Phys. **88**, 3448 (2000).
[33] A. Shik, H. Ruda, and E. Sargent, Nanotechnology **12**, 523 (2001).
[34] L. Bakueva, S. Musykhin, E. H. Sargent, H. E. Ruda, and A. Shik, in *Handbook of Organic-Inorganic Hybrid Materials and Nanocomposites*, edited by H. S. Nalwa (American Scientific Publishers, USA, 2003).
[35] V. M. Petrov, S. Wevering, M. P. Petrov, and E. Krätzig, Appl. Phys. B: Lasers Opt. **68**, 73 (1999).
[36] A. Grunnet-Jepsen, C. L. Thompson, and W. E. Moerner, J. Opt. Soc. Am. B **15**, 905 (1998).
[37] *Organic Electroluminescent Materials and Devices*, edited by S. Miyata and H. S. Nalwa (Gordon and Breach, New York, 1997).
[38] *Handbook of Physical Quantities*, edited by I. S. Grigoriev and E. Z. Meilikhov (Chemical Rubber, Boca Raton, 1997).
[39] A. C. Arango, S. A. Carter, and P. J. Brock, Appl. Phys. Lett. **74**, 1698 (1999).